Phys Chem Minerals (2004) 31: 278–287
DOI 10.1007/s00269-004-0385-z

ORIGINAL PAPER

A. Nakatsuka · H. Ueno · N. Nakayama · T. Mizota
H. Maekawa

Single-crystal X-ray diffraction study of cation distribution in $MgAl_2O_4$–$MgFe_2O_4$ spinel solid solution

Received: 17 April 2003 / Accepted: 12 January 2004

Abstract Synthesis experiments in the system $MgAl_2O_4$–$MgFe_2O_4$ [$MgAl_{2-x}Fe_xO_4$ ($0 \le x \le 2$)] were carried out using a PbF_2 flux. The crystalline products synthesized in the compositional range of $0.6 < x \le 1.2$ consisted of two spinel phases, whereas those synthesized in the compositional ranges of $0.0 \le x \le 0.6$ and $1.2 < x \le 2.0$ crystallized as single spinel phases. Structure refinements of the spinel single crystals, which grew in the ranges of $0.0 \le x \le 0.6$ and $1.2 < x \le 2.0$, show that the degree of randomness of cation distribution between A and B sites increases as x approaches the two-phase region. This means that the degree of the size mismatch among Mg^{2+}, Fe^{3+} and Al^{3+} occupying each equivalent mixing site increases as x approaches the two-phase region. Consequently, if the coexistence of two spinels observed in the intermediate compositions reveals the existence of a miscibility gap at low temperatures, this increase in the degree of the size mismatch among the three cations is suggested as a factor of energetic destabilization to form the miscibility gap.

Keywords Spinel · Solid solution · Cation distribution · Miscibility gap · Single-crystal X-ray diffraction

Introduction

Oxide spinels (TM_2O_4) have attracted great attention in the field of Earth science because of their importance as constituent minerals in many igneous and metamorphic rocks. The crystal structure of spinel belongs to the space group $Fd\bar{3}m$ with cations at Wyckoff positions 8*a* (1/8, 1/8, 1/8) and 16*d* (1/2, 1/2, 1/2) and oxygens at 32*e* (*u*, *u*, *u*). The positional parameter of the oxygens is conventionally called *u* parameter. The crystal structure is defined only by the *u* parameter and the lattice parameter (a_0). The structural formula of spinels can be expressed as $^{IV}(T_{1-i}M_i)^{VI}[T_iM_{2-i}]O_4$, where $^{IV}( )$ and $^{VI}[ ]$ represent the tetrahedral (A site; 8*a*) and the octahedral sites (B site; 16*d*), respectively; *i* is called the inversion parameter. The cation distributions of spinels are classified into normal ($i = 0$), inverse ($i = 1$) or intermediate ($0 < i < 1$). The spinel compounds with $0 \le i < 2/3$ and $2/3 < i \le 1$ are conventionally assigned to normal spinels and inverse spinels, respectively; the *i* value of 2/3 means that cations are randomly distributed between A and B sites.

Many pairs of oxide spinels form solid solutions between normal spinel end members (e.g. $MgAl_2O_4$–$ZnAl_2O_4$; Petrova et al. 1997), between inverse spinel end members (e.g. Fe_3O_4–$MgFe_2O_4$; Katayama and Iseda 2002) or between normal and inverse spinel end members (e.g. $MgAl_2O_4$–$MgFe_2O_4$; Sharma et al. 1973). In particular, some solid solutions between a normal and an inverse spinel end member show significantly non-linear variation of lattice parameters with composition (Robbins et al. 1971; Sharma et al. 1973), and a solvus may develop at low temperatures (Allen 1964, 1966; Sharma et al. 1973; Katayama et al. 1980; O'Neill and Navrotsky 1984). The system $MgAl_2O_4$–$MgFe_2O_4$ has been suggested as one of such examples (Kwestroo 1959; Allen 1964, 1966; Ulmer 1969; Sharma et al. 1973), but there has been some controversy as to the solvus relation in this system. Kwestroo (1959) found two spinels coexisting along the stoichiometric $MgAl_2O_4$–$MgFe_2O_4$ join at 1400 °C; Ulmer (1969) checked this result at 1300 °C and confirmed the coexistence of two spinels. On the other hand, Allen (1964, 1966) reported that the solvus exists below 1000 °C. Subsequently, Sharma et al. (1973) concluded from hydrothermal syntheses that the existence of the solvus in the system $MgAl_2O_4$–$MgFe_2O_4$

A. Nakatsuka (✉) · H. Ueno · N. Nakayama
T. Mizota
Department of Advanced Materials Science and Engineering, Faculty of Engineering, Yamaguchi University, Ube, Yamaguchi 755-8611, Japan
e-mail: tuka@po.cc.yamaguchi-u.ac.jp
Tel: +81-836-85-9651
Fax: +81-836-85-9601

H. Maekawa
Department of Metallurgy, Graduate School of Engineering, Tohoku University, Sendai, Miyagi 980-8579, Japan

is inconclusive, but, if the miscibility gap is present, the critical temperature of the solvus is below 950 °C under 7 kb and reduces to still lower temperatures under atmospheric pressure.

Cation distributions in solid solution contribute to the free energy of mixing (O'Neill and Navrotsky 1984). Therefore, if the miscibility gap exists in the system $MgAl_2O_4$–$MgFe_2O_4$, its formation will be closely related to cation distribution in $MgAl_2O_4$–$MgFe_2O_4$ spinel solid solution. Despite such an importance, the compositional dependence of cation distribution in this spinel solid solution has not yet been investigated in detail. In the present study, the single crystals of $MgAl_2O_4$–$MgFe_2O_4$ spinel solid solution are synthesized using the flux method, in order to grow the crystals at low temperatures where the existence of the miscibility gap can be expected. The synthesized single crystals are examined using single-crystal X-ray diffraction techniques, and the crystal chemistry of $MgAl_2O_4$–$MgFe_2O_4$ spinel solid solution is discussed with special attention to the compositional dependence of cation distribution.

Experiments and analyses

Sample preparation

The synthesis experiments in the system $MgAl_2O_4$–$MgFe_2O_4$ [$MgAl_{2-x}Fe_xO_4$ ($0 \le x \le 2$)] were carried out using a PbF_2 flux. Special grade reagents (99.99%) of MgO, α-Al_2O_3 and α-Fe_2O_3 were used as starting materials and mixed together with the PbF_2 flux in the molar ratio MgO : α-Al_2O_3 : α-Fe_2O_3 : $PbF_2 = 2 : (2-x) : x : 18$. This mixture was placed in a 30-cm^3 platinum crucible and heated slowly to 1200 °C. Then, the melt of the mixture was cooled at rates of 5 °C h^{-1} from 1200 to 700 °C and of 10 °C h^{-1} from 700 to 300 °C. Subsequently, the heating was turned off and the samples were removed from the furnace at room temperature. During the temperature control, the temperature stability in the furnace was kept within ±1 °C.

To identify the synthesized crystalline products, the powder X-ray diffraction (PXD) measurements were carried out at room temperature (23 °C) with a Rigaku RINT2200 powder X-ray diffractometer operated at 40 kV and 30 mA. The graphite-monochromatized Cu Kα radiation ($\lambda = 1.54184$ Å) was used for the measurements, and the PXD patterns were measured at a scan speed of 2° min^{-1}. The chemical analyses of the synthesized crystalline products were performed using a JEOL JCMA-733II electron microprobe analyzer (EPMA) operated at a 15-kV acceleration voltage and a 20-nA beam current. The products were mounted with epoxy and polished for EPMA analyses. The standard materials for the quantitative analyses of the elements Mg, Fe and Al were Mg_2SiO_4, α-Fe_2O_3 and α-Al_2O_3, respectively.

Some of the synthesized crystalline products crystallized as single crystals of $MgAl_{2-x}Fe_xO_4$ spinels, whose crystal sizes varied between 0.2 and 1.0 mm for the different compositions. The EPMA analyses confirmed compositional homogeneity of the synthesized single crystals, and their analytical results are given in Table 1. Neither Pb^{2+} nor F^-, which are components of flux, was detected in the single crystals, and their compositions showed no significant deviation from the ideal cation ratio of Mg^{2+}: (Fe^{3+} + Al^{3+}) = 1 : 2. Therefore we assume the single crystals to be stoichiometric, and their chemical compositions were determined to be $x = 0.00$, 0.04, 0.09, 0.23, 0.47, 0.59, 1.21, 1.53, 1.77 and 2.00.

Single-crystal X-ray diffraction intensity measurements

The spinel single crystals selected for single-crystal X-ray diffraction intensity measurements were ground into spheres of 0.107–0.190 mm in diameter (Table 2). The intensity data and lattice parameters of each single crystal were measured at room temperature (23 °C) using a Rigaku AFC-5S four-circle diffractometer operated at 45 kV and 30 mA. Mo Kα radiation ($\lambda = 0.71069$ Å) monochromatized by pyrolytic graphite was used for the measurements. The lattice parameters of all crystals were determined by the least-squares method using the 2θ values of the same 25 reflections in the range $40° \le 2\theta \le 50°$. A silicon single crystal was used as a standard material of the lattice-

Table 1 EPMA analyses

	$x = 0.00$	$x = 0.04$	$x = 0.09$	$x = 0.23$	$x = 0.47$
wt%					
MgO	28.0(1)	27.8(1)	27.6(1)	27.0(1)	25.8(1)
Al_2O_3	70.9(2)	69.0(2)	66.8(2)	60.6(2)	49.8(2)
Fe_2O_3	–	2.4(1)	4.9(2)	12.1(2)	24.1(3)
Total	98.9	99.2	99.3	99.7	99.7
Cationic molar ratio (for four O)					
Mg^{2+}	1.000(5)	0.999(5)	1.000(5)	1.000(5)	1.001(5)
Al^{3+}	2.000(6)	1.958(7)	1.911(6)	1.774(6)	1.528(6)
Fe^{3+}	–	0.043(2)	0.089(3)	0.226(4)	0.472(6)
Total	3.000	3.000	3.000	3.000	3.001
	$x = 0.59$	$x = 1.21$	$x = 1.53$	$x = 1.77$	$x = 2.00$
wt%					
MgO	25.6(2)	22.8(2)	21.9(2)	20.6(2)	20.6(2)
Al_2O_3	44.9(2)	22.2(1)	12.7(1)	6.3(1)	–
Fe_2O_3	29.9(3)	54.3(5)	65.3(5)	72.6(6)	79.7(6)
Total	100.4	99.3	99.9	99.5	100.3
Cationic molar ratio (for four O)					
Mg^{2+}	1.009(9)	1.011(11)	1.013(11)	0.992(12)	1.018(12)
Al^{3+}	1.399(6)	0.778(4)	0.464(4)	0.240(3)	–
Fe^{3+}	0.594(7)	1.214(11)	1.527(11)	1.766(14)	1.988(16)
Total	3.002	3.003	3.004	2.998	3.006

Table 2 Crystallographic data, data collection and refinement parameters

	$x = 0.00$	$x = 0.04$	$x = 0.09$	$x = 0.23$	$x = 0.47$
Temperature (°C)	23	23	23	23	23
a_0 (Å)	8.0861(3)	8.0926(3)	8.0993(4)	8.1211(4)	8.1576(3)
V (Å^3)	528.7(1)	530.0(1)	531.3(1)	535.6(1)	542.9(1)
Space group	$Fd\bar{3}m$	$Fd\bar{3}m$	$Fd\bar{3}m$	$Fd\bar{3}m$	$Fd\bar{3}m$
Crystal size (mm, diameter)	0.107	0.130	0.165	0.160	0.160
Radiation used	Mo Kα	Mo Kα	Mo Kα	Mo Kα	Mo Kα
μ (cm^{-1})	11.62	13.61	16.09	22.94	34.45
μr	0.062	0.088	0.133	0.184	0.276
No. of measured reflections	395	397	397	402	408
No. of observed independent reflections with $\|F_o\| \geq 3\sigma(\|F_o\|)$ after averaging equivalent reflections	132	133	123	109	119
No. of reflections within $0.36 \leq \sin\theta/\lambda \leq 0.70$ used in step II	40	39	37	35	40
R_{int} (%)	0.50	0.87	1.61	0.87	1.05
R (%)	2.26	2.71	2.29	2.10	2.16
R_w (%)	1.34	1.89	1.97	1.56	1.70
	$x = 0.59$	$x = 1.21$	$x = 1.53$	$x = 1.77$	$x = 2.00$
Temperature (°C)	23	23	23	23	23
a_0 (Å)	8.1817(7)	8.2796(5)	8.3252(4)	8.3422(5)	8.3600(4)
V (Å^3)	547.7(2)	567.6(2)	577.0(1)	580.6(1)	584.3(1)
Space group	$Fd\bar{3}m$	$Fd\bar{3}m$	$Fd\bar{3}m$	$Fd\bar{3}m$	$Fd\bar{3}m$
Crystal size (mm, diameter)	0.167	0.160	0.145	0.160	0.190
Radiation used	Mo Kα	Mo Kα	Mo Kα	Mo Kα	Mo Kα
μ (cm^{-1})	40.00	67.79	81.50	92.05	101.98
μr	0.334	0.542	0.591	0.736	0.969
No. of measured reflections	411	420	437	437	437
No. of observed independent reflections with $\|F_o\| \geq 3\sigma(\|F_o\|)$ after averaging equivalent reflections	115	129	126	129	138
No. of reflections within $0.36 \leq \sin\theta/\lambda \leq 0.70$ used in step II	36	36	36	35	–
R_{int} (%)	1.56	0.90	2.03	1.51	1.00
R (%)	1.90	2.48	2.60	2.53	2.51
R_w (%)	1.64	1.82	1.89	2.00	1.97

parameter determinations. Reflection intensities in the range $2° \leq 2\theta \leq 100°$, corresponding to $0.02 \leq \sin\theta/\lambda \leq 1.08$, were measured in the ω scan mode. All the intensities were collected at a scan speed of 2° min^{-1}. The intensity data were corrected for Lorentz-polarization factors and spherical absorption effects ($\mu r = 0.062$–0.969 for Mo Kα radiation). The total number of measured reflections for the different single crystals varied between 395 and 437. The number of observed independent reflections with $|F_o| \geq 3\sigma(|F_o|)$ after averaging the equivalent reflections varied between 109 and 138 for the different single crystals, and these reflections were used for the structure refinements. Internal residuals of the equivalent reflections (R_{int} in Table 2) varied between 0.50 and 2.03% for the different single crystals.

Structure refinements

The structure refinements were carried out by minimizing the residual factor $\sum w(|F_o| - |F_c|)^2$ using a full-matrix least-squares program RADY (Sasaki 1987), where $w = 1/\sigma^2(|F_o|)$. Scattering factors for Mg^{2+}, Al^{3+}, Fe^{3+} (International tables for X-ray crystallography 1974) and O^{2-} (Tokonami 1965) were used for the structure refinements. The correction terms for anomalous dispersion of each element were also taken from the International tables for X-ray crystallography (1974). In the refinements, an anisotropic thermal motion model was applied to the displacement parameters. Furthermore, a correction of isotropic extinction effects (type I) was performed (Becker and Coppens 1974a, b).

In the $MgAl_{2-x}Fe_xO_4$ spinel solid solution, Mg^{2+}, Al^{3+} and Fe^{3+} can occupy both A and B sites, as shown in the following structural formula:

$$^{IV}(Mg_{1-p-q}Al_pFe_q)^{VI}[Mg_{(p+q)/2}Al_{(2-p-x)/2}Fe_{(x-q)/2}]_2O_4 \ , \quad (1)$$

where $^{IV}()$ and $^{VI}[\ ]$ represent A and B sites, respectively; p and q are occupancy parameters of Al^{3+} and Fe^{3+} on the A site, respectively; x is the composition (Fe^{3+} content) of the solid solution determined by EPMA. In principle, we can simultaneously determine the site occupancies of Mg^{2+}, Al^{3+} and Fe^{3+} on both A and B sites by constraining the occupancy parameters on the basis of structural formula (1). This is because the two independent occupancy parameters p and q can be uniquely determined from the following two Eqs. (2) and (3):

$$f_A = (1 - p - q)f_{Mg} + pf_{Al} + qf_{Fe} \ , \quad (2)$$

$$f_B = \frac{p+q}{2}f_{Mg} + \frac{2-p-x}{2}f_{Al} + \frac{x-q}{2}f_{Fe} \ , \quad (3)$$

where the composition x is a fixed value determined by EPMA; f_A and f_B are the mean scattering powers from A and B sites, respectively; f_{Mg}, f_{Al} and f_{Fe} are the scattering factors of Mg^{2+}, Al^{3+} and Fe^{3+}, respectively. However, the determination of the occupancy parameter p, related to the Al^{3+}/Mg^{2+} ratios on A and B sites, involves large uncertainties because of the similarity of f_{Mg} and f_{Al}. Therefore, in order to determine the occupancy parameter p as exactly as possible, we carried out the structure refinements under the above constraints for the occupancy parameters in accordance with the following procedures (steps I–III), except for the Al-free sample, i.e. $MgFe_2O_4$ ($x = 2$).

Step I: First, all the variable parameters (the occupancy parameters p and q, u parameter, displacement parameters, scale factor and extinction parameter) were refined on the basis of all the observed reflection data. The p values refined here have large uncertainties, but the uncertainties do not greatly influence the

refinements of the q values, u parameters and displacement parameters, because f_{Mg} and f_{Al} are similar to each other.

Step II: Secondly, to reduce the uncertainties of the occupancy parameter p, it was refined again together with scale factor and extinction parameter, using only reflections within the range $0.36 \le \sin\theta/\lambda \le 0.70$ (shaded area in Fig. 1) in which the difference between f_{Mg} and f_{Al} is large. Since the usage of reflections only within this range is suitable only for reducing uncertainties of p, other structural parameters (q, u parameter and displacement parameters) were fixed at their values obtained in step I. The number of reflections included in this region varied between 35 and 40 for the different single crystals (Table 2) and is more than ten times as many as that of the parameters (p, scale factor and extinction parameter) varied in this step; thus, this region gives the number of reflections enough to refine these three parameters reliably.

Step III: Finally, the u parameter, displacement parameters, scale factor and extinction parameter were refined once more on the basis of all the observed reflection data with the occupancy parameters p and q fixed at the values determined in steps II and I, respectively. In these final refinements, R and R_w factors varied between 1.90 and 2.71% and between 1.34 and 2.00% for the different datasets, respectively (Table 2).

The final u parameters and displacement parameters, determined in step III, are listed in Table 3 together with selected interatomic distances. The final occupancy parameters, based on the q values determined in step I and the p values determined in step II, are given in Table 4. The standard deviations for the refined structural parameters in Tables 3 and 4 are the same as those estimated for the final values of each parameter. Consequently, the standard deviations for the interatomic distances in Table 3 are based on those for the u parameters refined in step III and the lattice parameters.

^{27}Al MAS NMR measurements

The site occupancies for the Fe^{3+}-free sample, i.e. $MgAl_2O_4$ spinel ($x = 0$), were also examined by ^{27}Al MAS NMR. The ^{27}Al MAS NMR spectra were measured with a Bruker MSL-300 spectrometer operated at 78.205 MHz and with a Bruker high-speed MAS probe operated at a spinning speed of 15 kHz. The chemical shift was referenced to a 1 mol l^{-1} aqueous solution of $Al(NO_3)_3$. An appropriate output power for the excitation pulse was set using an attenuator, where the $\pi/2$ pulse width determined from the ^{27}Al NMR signal of this aqueous solution was 14 μs. The ^{27}Al MAS NMR spectra of the present $MgAl_2O_4$ spinel were measured using a 0.6-μs pulse width (corresponding to $\pi/16$ pulse) and a 10-s delay between excitation pulses.

The ^{27}Al MAS NMR spectra of $MgAl_2O_4$ spinel synthesized in the present study are shown in Fig. 2. The spectra contain a small peak at about 70 ppm and a main doublet peak at about 0 ppm, consistent with those of the previous studies (Gobbi et al. 1985; Dupree et al. 1986; Wood et al. 1986; Millard et al. 1992; Maekawa et al. 1997; Ito et al. 2000). The former peak corresponds to the A-site Al and the latter to the B-site Al, and the relative amounts of the A-site Al and the B-site Al can be directly obtained from each peak area. Thus, the site occupancies of Al^{3+} and Mg^{2+} can be calculated under the constraint of the structural formula $^{IV}(Mg_{1-i}Al_i)^{VI}[Mg_iAl_{2-i}]O_4$, and the result is given in Table 5.

Validity of the refined occupancy parameters

A good test to assess the validity of the refined occupancy parameters is to examine whether the bond lengths fall on a line against the mean cation sizes calculated from the refined occupancy parameters and the effective ionic radii (Shannon 1976). In the present study, the bond lengths on both the A and B sites vary linearly within the errors with the mean cation size (Fig. 3). Moreover, the refined occupancies of the present $MgAl_2O_4$ spinel (Table 4) agree well with those obtained from the ^{27}Al MAS NMR spectra (Table 5). Thus, these two independent checks for the refined occupancies demonstrate that the present structure refinements provided reliable occupancy parameters. Hence, it follows that the refined displacement parameters, correlated with occupancy parameters, are also suitable.

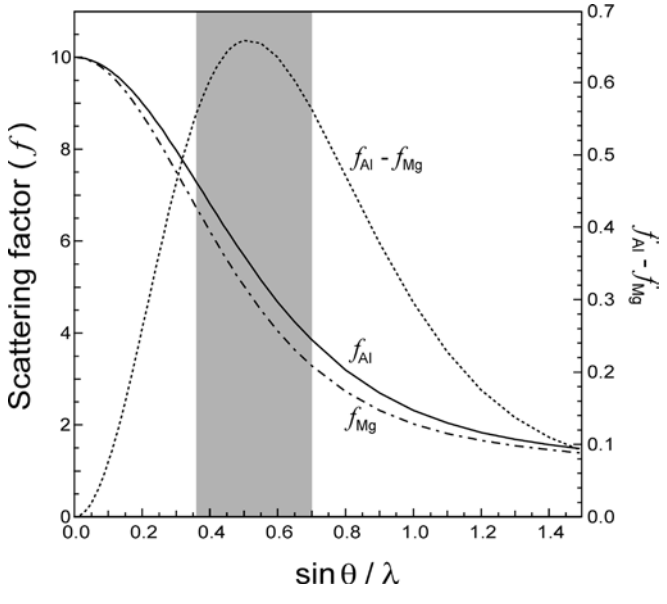

Fig. 1 Ionized scattering factor curves. *Solid line* and *dashed-dotted line* are the scattering factors of Al^{3+} (f_{Al}) and Mg^{2+} (f_{Mg}), respectively. *Dotted line* represents $f_{Al}-f_{Mg}$. *Shaded area* displays the $\sin\theta/\lambda$ range of the reflections used for the structure refinements in step II ($0.36 \le \sin\theta/\lambda \le 0.70$)

Results and discussion

Two-phase region

Figure 4 shows the selected PXD patterns of the synthesized crystalline products. The PXD patterns of the crystalline products synthesized from the initial compositions in the ranges of $0.0 \le x \le 0.6$ and $1.2 < x \le 2.0$ can be indexed as single spinel phases, whereas those in the range of $0.6 < x \le 1.2$ can be indexed as two spinel phases (Fig. 4). Although the diffraction peaks of the sample with the initial composition $x = 1.3$ seem to be somewhat broader than those of other single phases, we regarded this sample as a single phase for the following reasons: the shapes of the peaks are symmetric; all the crystal grains in this sample analyzed with EPMA have the same chemical composition and no evidence for two phases could be found. The single crystals of the spinels crystallized in the single-phase regions of $0.0 \le x \le 0.6$ and $1.2 < x \le 2.0$. They have the positive excess volume as observed in Fig. 5, which may reflect the excess energy of mixing involved in the formation of miscibility gap.

To gain conclusive evidence that the coexistence of two spinels observed here reveals the existence of a miscibility gap at low temperatures, we synthesized the

Table 3 Refined oxygen coordinates u, anisotropic displacement parameters β_{ij} ($\times 10^5$), equivalent isotropic displacement parameters B_{eq} (Å^2) and selected interatomic distances (Å)

	$x = 0.00$	$x = 0.04$	$x = 0.09$	$x = 0.23$	$x = 0.47$
u	0.2622(1)	0.2623(1)	0.2619(1)	0.2617(1)	0.2610(1)
β_{11} (A site)[a]	210(2)	189(2)	235(2)	199(2)	196(2)
β_{11} (B site)[b]	172(1)	167(1)	229(2)	169(1)	190(1)
β_{12} (B site)[b]	−10(1)	−5(1)	−6(2)	−5(1)	−6(1)
β_{11} (Oxygen site)[b]	256(2)	252(2)	326(3)	271(2)	306(2)
β_{12} (Oxygen site)[b]	16(2)	7(2)	3(2)	−1(2)	−13(2)
B_{eq} (A site)[c]	0.550(2)	0.495(2)	0.617(2)	0.526(2)	0.521(1)
B_{eq} (B site)[c]	0.451(1)	0.438(1)	0.602(1)	0.447(1)	0.504(1)
B_{eq} (Oxygen site)[c]	0.671(2)	0.660(2)	0.855(2)	0.714(2)	0.815(2)
A–O	1.921(1)	1.924(1)	1.920(1)	1.922(1)	1.922(1)
B–O	1.928(1)	1.929(1)	1.934(1)	1.940(1)	1.953(1)
$(O\ldots O)_{tetra}$[d]	3.137(1)	3.142(2)	3.135(2)	3.139(2)	3.139(2)
$(O\ldots O)_{shared}$[e]	2.581(1)	2.580(2)	2.592(2)	2.604(2)	2.629(2)
$(O\ldots O)_{unshared}$[f]	2.866(1)	2.868(2)	2.870(2)	2.877(2)	2.890(2)
	$x = 0.59$	$x = 1.21$	$x = 1.53$	$x = 1.77$	$x = 2.00$
u	0.2603(1)	0.2588(1)	0.2578(2)	0.2570(2)	0.2573(2)
β_{11} (A site)[a]	230(2)	204(1)	195(1)	202(1)	237(2)
β_{11} (B site)[b]	231(1)	215(1)	207(1)	220(1)	250(1)
β_{12} (B site)[b]	−8(1)	−10(1)	−10(2)	−12(2)	−13(1)
β_{11} (Oxygen site)[b]	367(3)	335(3)	289(3)	285(3)	281(2)
β_{12} (Oxygen site)[b]	−13(3)	−21(3)	−24(4)	−20(4)	−2(4)
B_{eq} (A site)[c]	0.616(1)	0.559(1)	0.541(1)	0.563(1)	0.662(1)
B_{eq} (B site)[c]	0.620(1)	0.591(1)	0.573(1)	0.613(1)	0.700(1)
B_{eq} (Oxygen site)[c]	0.982(2)	0.919(2)	0.802(2)	0.794(2)	0.785(2)
A–O	1.918(1)	1.918(1)	1.915(1)	1.907(1)	1.915(1)
B–O	1.965(1)	2.000(1)	2.018(1)	2.029(1)	2.031(1)
$(O\ldots O)_{tetra}$[d]	3.132(2)	3.133(2)	3.127(3)	3.115(3)	3.128(3)
$(O\ldots O)_{shared}$[e]	2.654(2)	2.722(2)	2.760(3)	2.784(3)	2.784(3)
$(O\ldots O)_{unshared}$[f]	2.898(2)	2.931(2)	2.946(3)	2.952(3)	2.958(3)

[a] $\beta_{11} = \beta_{22} = \beta_{33}$, $\beta_{12} = \beta_{13} = \beta_{23} = 0$
[b] $\beta_{11} = \beta_{22} = \beta_{33}$, $\beta_{12} = \beta_{13} = \beta_{23}$
[c] $B_{eq} = (4/3)\Sigma_i\Sigma_j\beta_{ij}a_i.a_j$.
[d] Edge length of the tetrahedron about the A site
[e] Shared edge length of the octahedron about the B site
[f] Unshared edge length of the octahedron about the B site

Table 4 Refined occupancy parameters

Composition	Site	Occupancy parameters		
		Fe^{3+}	Mg^{2+}	Al^{3+}
$x = 0.00$	A	–	0.78	0.22(3)
	B	–	0.11	0.89
$x = 0.04$	A	0.01(2)	0.73	0.26(1)
	B	0.01	0.14	0.85
$x = 0.09$	A	0.03(2)	0.73	0.24(1)
	B	0.03	0.13	0.84
$x = 0.23$	A	0.11(2)	0.62	0.27(1)
	B	0.06	0.19	0.75
$x = 0.47$	A	0.21(2)	0.56	0.24(1)
	B	0.13	0.22	0.65
$x = 0.59$	A	0.26(2)	0.61	0.13(1)
	B	0.16	0.20	0.64
$x = 1.21$	A	0.53(3)	0.38	0.09(1)
	B	0.34	0.31	0.35
$x = 1.53$	A	0.66(4)	0.28	0.05(1)
	B	0.43	0.36	0.21
$x = 1.77$	A	0.81(4)	0.19	0.00(1)
	B	0.48	0.41	0.11
$x = 2.00$	A	0.854(6)	0.146	–
	B	0.573	0.427	–

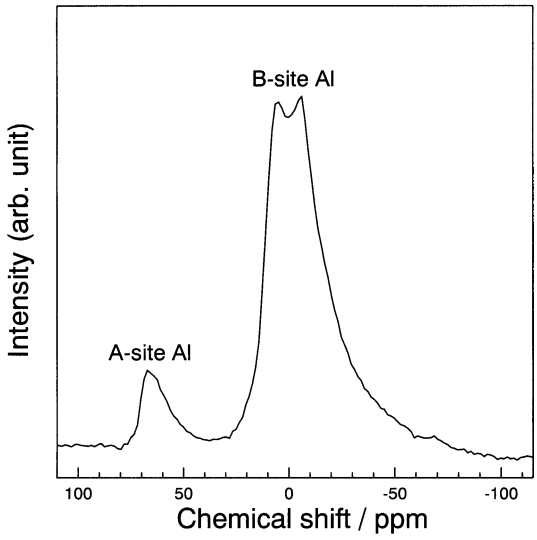

Fig. 2 ^{27}Al MAS NMR spectra of $MgAl_2O_4$ spinel single-crystal synthesized in the present study

Table 5 Occupancy parameters of $MgAl_2O_4$ spinel obtained from NMR spectra

	Relative intensity of NMR peak (%)	Occupancies
A site		
Mg^{2+}	–	0.796
Al^{3+}	10.2(8)	0.204 (16)
B site		
Mg^{2+}	–	0.102
Al^{3+}	89.8(8)	0.898 (8)

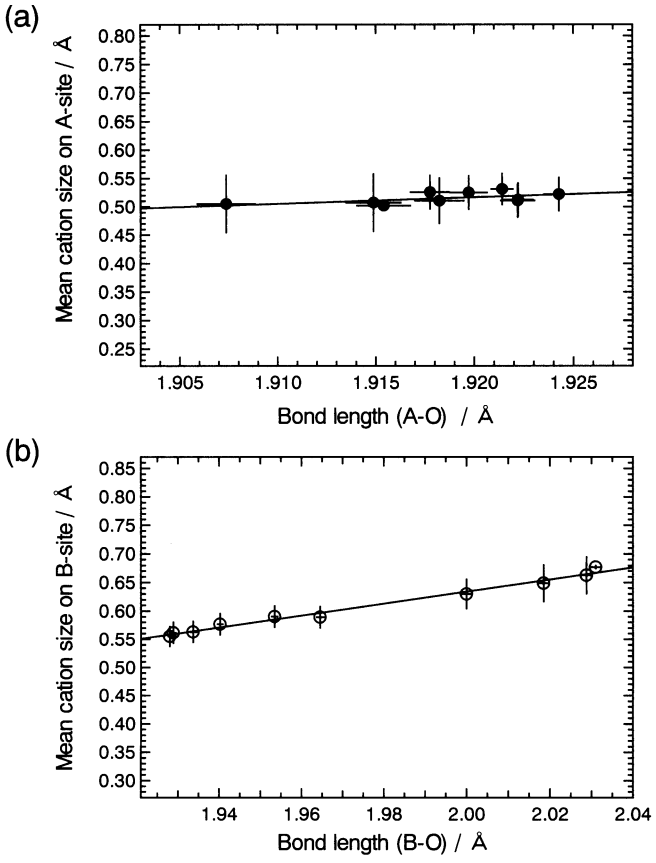

Fig. 3a, b The relationship between the mean cation size and the bond length; **a** A site, **b** B site. The mean cation size ($<r>$) is calculated from $<r> = P_{Fe} \cdot r_{Fe} + P_{Al} \cdot r_{Al} + P_{Mg} \cdot r_{Mg}$, where P_{Fe}, P_{Al} and P_{Mg} are the occupancy parameters of Fe^{3+}, Al^{3+} and Mg^{2+} determined by single-crystal X-ray diffraction, respectively; r_{Fe}, r_{Al} and r_{Mg} are the effective ionic radii (Shannon 1976) of Fe^{3+}, Al^{3+} and Mg^{2+}, respectively

powder samples of homogeneous solid solution at 1300 °C using a solid-state reaction and annealed these samples at 700 °C, lower than the possible critical temperature (950 °C) of solvus suggested by Sharma et al. (1973), for 30 days. Consequently, as shown in Fig. 6a and b, we failed to separate the homogeneous spinel solid solution into two spinels. However, this result does not exclude the possibility that a miscibility gap exists in the system $MgAl_2O_4$–$MgFe_2O_4$ because the kinetics of atomic diffusion is expected to be very slow at such low temperatures.

Compositional dependence of structural parameters

The variations of the occupancy parameters of Fe^{3+}, Al^{3+} and Mg^{2+} versus the composition (x) are shown in Fig. 7a, b and c, respectively. As shown in these figures, all the occupancy parameters vary monotonously, almost linearly, against x through the whole compositional range in the single-phase region. This indicates that the site distribution of each cation obeys the same mechanism in both $MgAl_2O_4$-rich ($0.0 \leq x \leq 0.6$) and $MgFe_2O_4$-rich ($1.2 < x \leq 2.0$) single-phase regions. Hence, the u parameter (Fig. 8), connected with cation distribution of spinels, also shows a monotonous variation against x and the tendency for its compositional dependence does not change between both single-phase regions.

Figure 9 shows the compositional dependence of the equivalent isotropic displacement parameters (B_{eq}). The B_{eq} values include the effects of both static and dynamic disorders; the static disorder is the configurational disorder, whereas the dynamic disorder arises from the thermal vibration of atoms. As the present B_{eq} values were determined at the same temperature (23 °C) for each sample, the compositional dependence of the B_{eq} values in Fig. 9 is considered to reflect the variation of the degree of configurational disorder versus x. Figure 9 proposes, therefore, that the degrees of configurational disorders of cations on A and B sites are hardly influenced by the variation of x, whereas that of oxygen increases greatly as x approaches the two-phase region. Thus, the sensibilities of the configurational disorders to the variation of x differ between oxygen and cations. This can be due to the difference in the degrees of freedom between the

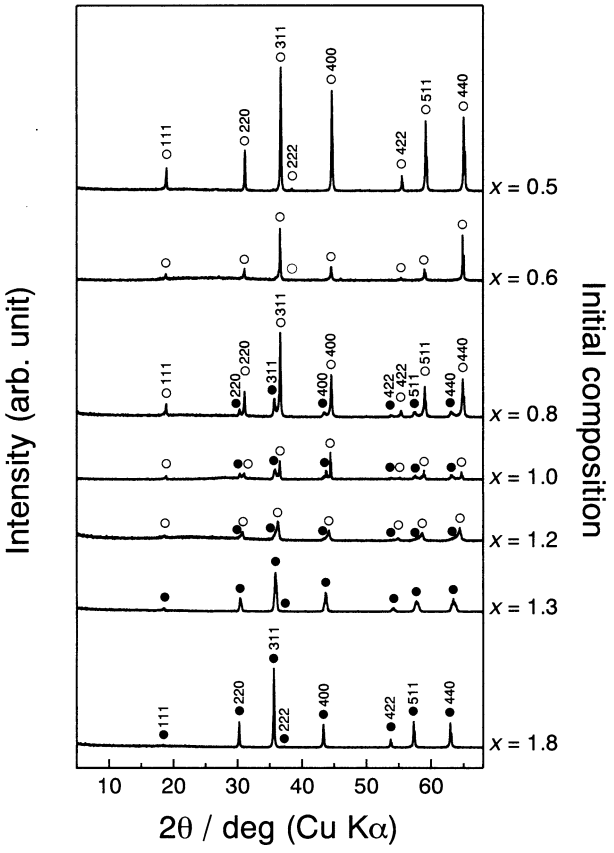

Fig. 4 Variation of powder X-ray diffraction patterns of the synthesized crystalline products versus the initial compositions in the sample preparation. *Open circles* represent the diffraction peaks from spinel solid solution with $MgAl_2O_4$-rich composition; *solid circles* are those from spinel solid solution with $MgFe_2O_4$-rich composition

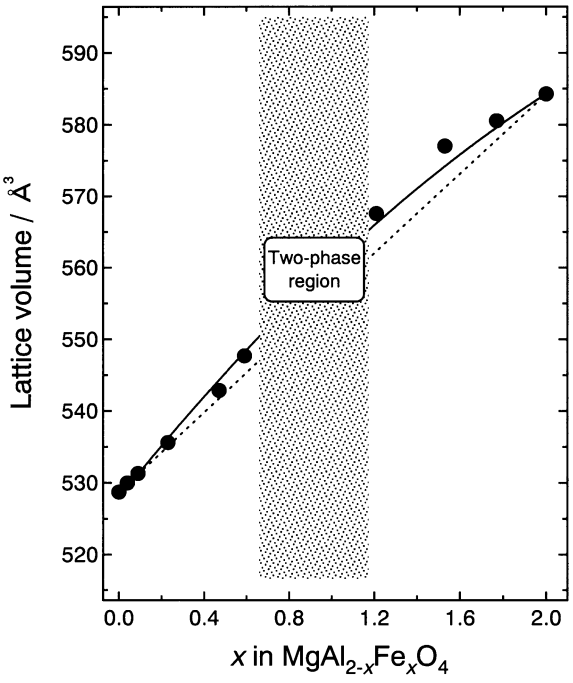

Fig. 5 The compositional dependence of lattice volume. *Dotted line* shows the variation expected from Vegard's law

atomic positions of oxygen and cations; the positional parameters of cations, 8*a* (1/8, 1/8, 1/8) for A site and 16*d* (1/2, 1/2, 1/2) for B site, have no degree of freedom, whereas that of oxygen, 32*e* (*u*, *u*, *u*), has the degree of freedom in the direction of $<111>$.

Cation distribution

We define the fractional parameter Q to estimate the site selectivity of the cations. On the basis of the above structural formula (1), the fractional parameters Q_{Fe}, Q_{Al} and Q_{Mg} for Fe^{3+}, Al^{3+} and Mg^{2+} are expressed as follows, respectively:

$$Q_{Fe} = Fe_{tetra}/Fe_{total} = q/x,$$

$$Q_{Al} = Al_{tetra}/Al_{total} = p/(2-x),$$

$$Q_{Mg} = Mg_{tetra}/Mg_{total} = 1-p-q \ ,$$

where Fe_{tetra}, Al_{tetra} and Mg_{tetra} are the contents of Fe^{3+}, Al^{3+} and Mg^{2+} occupying the A site, respectively; Fe_{total}, Al_{total} and Mg_{total} are the total contents of Fe^{3+}, Al^{3+} and Mg^{2+} in the solid solution, respectively. When $Q = 1/3$, the cations are randomly distributed between A and B sites because the cation ratio between A and B sites is 1 : 2; the cations dominantly occupy the A site when $Q > 1/3$ and the B site when $Q < 1/3$. The compositional dependence of the Q_{Fe}, Q_{Al} and Q_{Mg} values is shown in Fig. 10a, b and c, respectively. The Q_{Fe} value is nearly constant at about 0.44 in both $MgAl_2O_4$-rich and $MgFe_2O_4$-rich single-phase regions, which shows that Fe^{3+} dominantly occupies A site rather than B site at a constant ratio regardless of x (Fig. 10a). The Q_{Al} value is nearly constant at about 0.13 in both single-phase regions, which shows that Al^{3+} dominantly occupies B site rather than A site at a constant ratio regardless of x (Fig. 10b). On the other hand, the Q_{Mg} value decreases remarkably with increasing x, from 0.8 to 0.5 in the $MgAl_2O_4$-rich single-phase region and from 0.3 to 0.15 in the $MgFe_2O_4$-rich single-phase region; this shows that Mg^{2+} is dominantly distributed to the A site in the former region and the B site in the latter region (Fig. 10c).

These variations of Q_{Fe}, Q_{Al} and Q_{Mg} show that the selectivity of cations for the B site is getting stronger in the orders of $Mg^{2+} < Fe^{3+} < Al^{3+}$ in the $MgAl_2O_4$-rich single-phase region and $Fe^{3+} < Mg^{2+} < Al^{3+}$ in the $MgFe_2O_4$-rich single-phase region. Thus, Al^{3+} with the smallest size of these three cations ($r_{Al} < r_{Fe} < r_{Mg}$; Shannon 1976) has the most pronounced selectivity for the larger B site. In particular, the relation of site selectivity between Al and Mg is contradictory not only to the relation of cation size but also to that of elec-

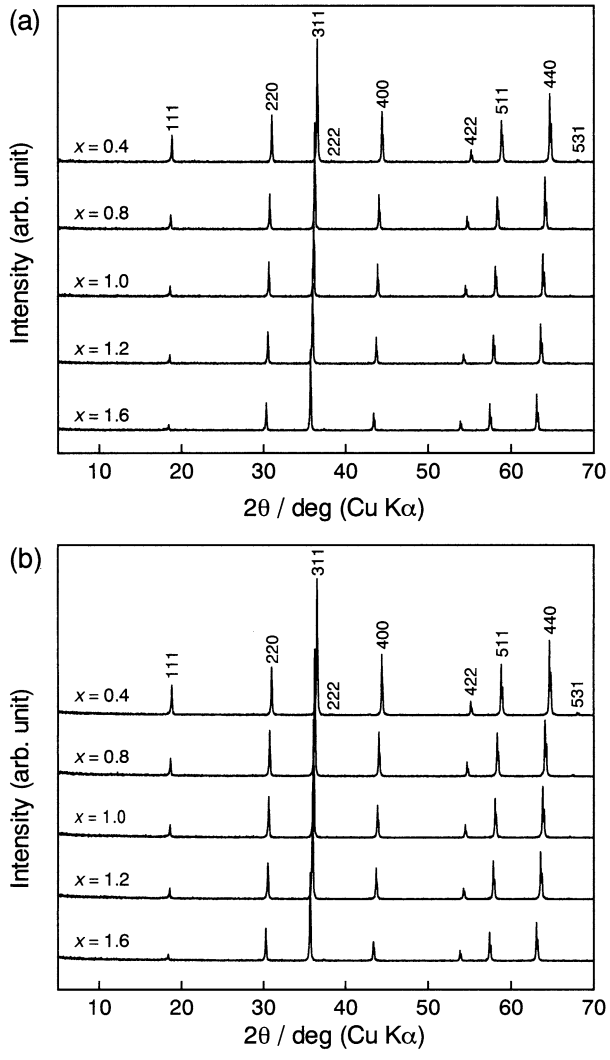

Fig. 6a, b Powder X-ray diffraction patterns of **a** $MgAl_2O_4$–$MgFe_2O_4$ spinel solid solution synthesized at 1300 °C using a solid-state reaction and **b** the samples annealed at 700 °C for 30 days

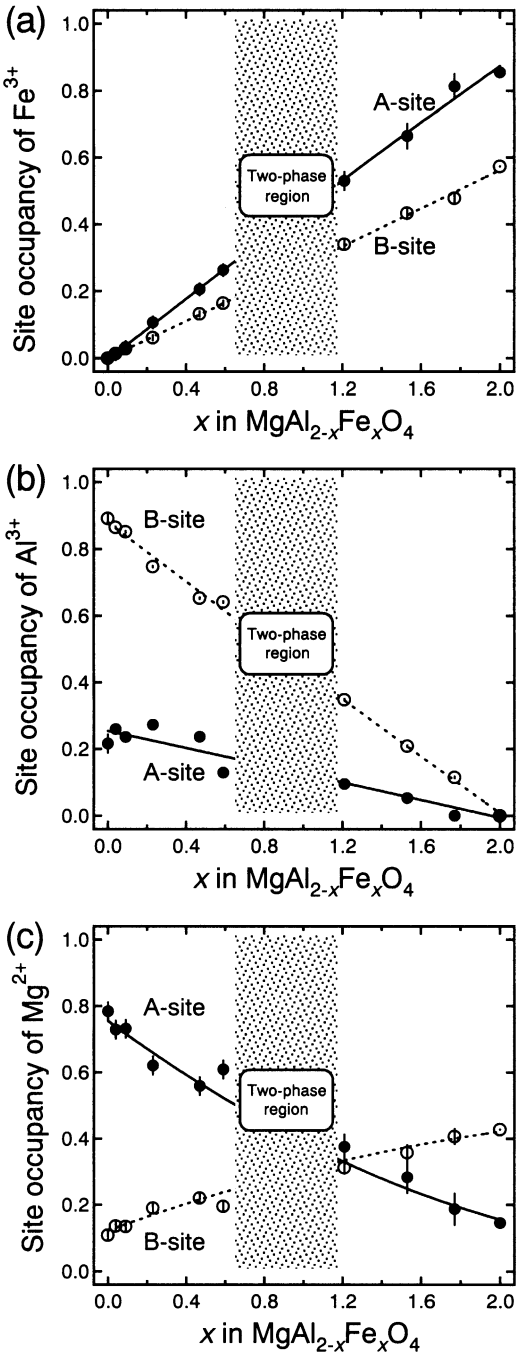

Fig. 7a–c Variations of the occupancy parameters of **a** Fe^{3+}, **b** Al^{3+} and **c** Mg^{2+} versus the composition (x). *Solid circles* and *open circles* represent the occupancy parameters of the cations on A and B sites, respectively. *Solid lines* and *dotted lines* represent the tendencies for the compositional dependence of the occupancy parameters of the cations on A and B sites, respectively

tronegativity ($\chi_{Mg} < \chi_{Al}$; Allred and Rochow 1958, Pauling 1960, Sanderson 1967). A strong selectivity of Al^{3+} for the B site has been also observed in $CoAl_2O_4$ and $FeAl_2O_4$ spinels (Greenwald et al. 1954; Toriumi et al. 1978; Porta and Anichini 1980; O'Neill 1994; Larsson et al. 1994; Harrison et al. 1998), although Co^{2+} and Fe^{2+} should prefer the B site more than Al^{3+} owing to ligand-field effects in addition to the effect of cation size.

A further notable feature of the cation distribution is that the degree of randomness of cation distribution between A and B sites depends mainly on that of the Mg^{2+} distribution and increases as x comes close to the two-phase region. This is led from the result that only Q_{Mg} depends remarkably on x in contrast to Q_{Fe} and Q_{Al} as described above and its value approaches 1/3 as x comes close to the two-phase region (Fig. 10c). Such an increase in the degree of randomness of cation distribution enhances the degree of size mismatch among Mg^{2+}, Fe^{3+} and Al^{3+} occupying each equivalent mixing site as x comes close to the two-phase region; this is reasonably consistent with the variation of configurational disorder of oxygen expected from Fig. 9. If the two-phase region observed in the present study reveals the existence of the miscibility gap at low temperatures,

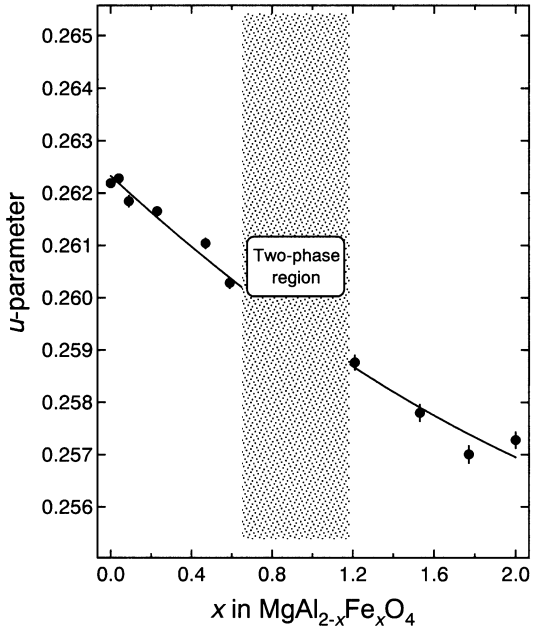

Fig. 8 The compositional dependence of *u* parameter

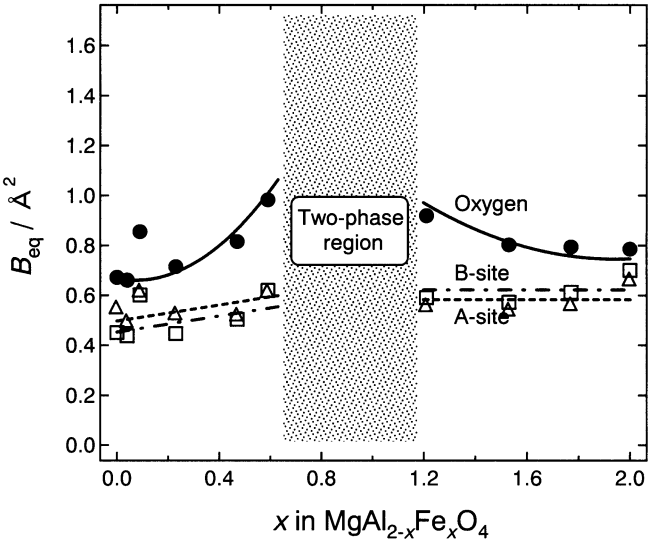

Fig. 9 The compositional dependence of the equivalent isotropic displacement parameters (B_{eq}). *Solid circles* Oxygen; *open triangles* A-site cation; *open squares* B-site cation. *Solid line*, *dotted line* and *dashed-dotted line* represent the tendencies for the compositional dependence of B_{eq} for oxygen, A-site cation and B-site cation, respectively. The standard deviations for each B_{eq} are less than the magnitudes of the symbols

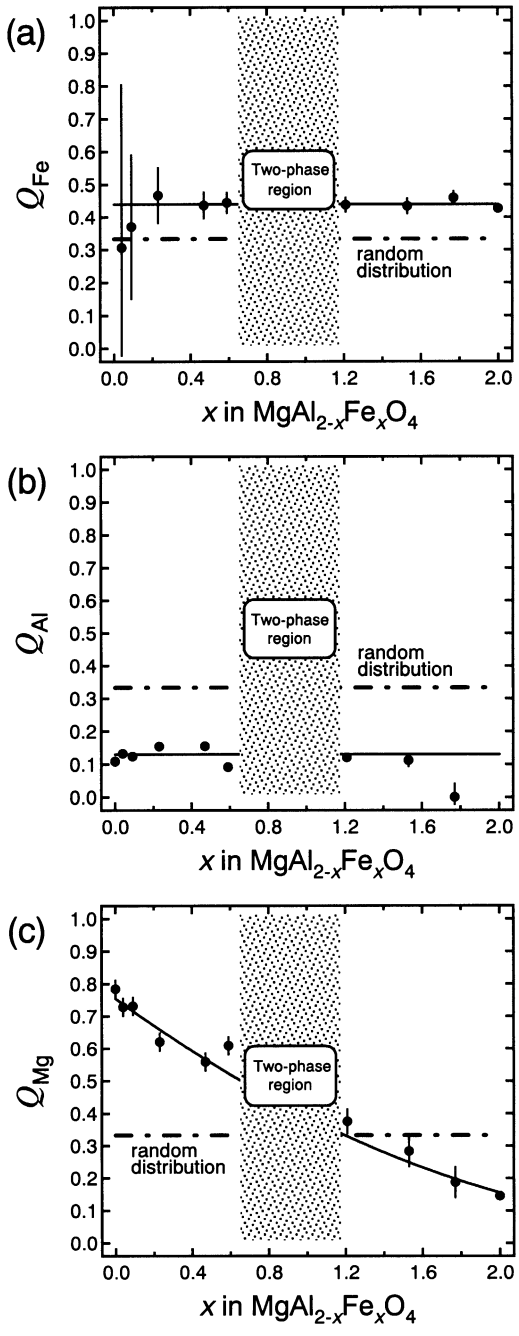

Fig. 10a–c The compositional dependence of the fractional parameters **a** Q_{Fe}, **b** Q_{Al} and **c** Q_{Mg}. *Dashed-dotted line* shows a completely random cation distribution between A and B sites

thus, this increase in the degree of the size mismatch among the three cations is suggested as a factor of energetic destabilization to form the miscibility gap. In particular, the difference in cation size is large enough between the largest Mg^{2+} and the smallest Al^{3+} of the three cations ($r_{Mg}-r_{Al} = 0.18$ Å for fourfold coordination and 0.185 Å for sixfold coordination; Shannon 1976). If the miscibility gap is present, therefore, the size mismatch between Mg^{2+} and Al^{3+} on each equivalent mixing site will play the most important role in its formation.

Acknowledgements The authors would like to thank Drs. Y. Shibata and M. Ohkawa of Hiroshima University for EPMA analyses. This work was partly supported by Grant-in-Aid for Scientific Research (no. 12740299) from the Ministry of Education, Culture, Sports, Science and Technology of the Japanese Government.

References

Allen WC (1964) Solid solution in the refractory magnesium spinels. PhD Thesis. The State University, New Brunswick

Allen WC (1966) An X-ray method for defining composition of a magnesium spinel. Am Mineral 51: 239–243

Allred AL, Rochow EG (1958) A scale of electronegativity based on electrostatic force. J Inorg Nucl Chem 5: 264–268

Becker PJ, Coppens P (1974a) Extinction within the limit of validity of the Darwin transfer equations. I. General formalisms for primary and secondary extinction and their application to spherical crystals. Acta Crystallogr (A)30: 129–147

Becker PJ, Coppens P (1974b) Extinction within the limit of validity of the Darwin transfer equations. II. Refinement of extinction in spherical crystals of SrF_2 and LiF. Acta Crystallogr (A)30: 148–153

Dupree R, Lewis MH, Smith ME (1986) A study of the vacancy distribution in non-stoichiometric spinels by magic-angle spinning NMR. Philosoph Mag (A)53: L17–L20

Gobbi GC, Christoffersen R, Otten MT, Miner B, Buseck PR, Kennedy GJ, Fyfe CA (1985) Direct determination of cation disorder in $MgAl_2O_4$ spinel by high-resolution ^{27}Al magic-angle-spinning NMR spectroscopy. Chem Lett 771–774

Greenwald S, Pickart SJ, Grannis FH (1954) Cation distribution and g factors of certain spinels containing Ni^{++}, Mn^{++}, Co^{++}, Al^{+++}, Ga^{+++}, and Fe^{+++}. J Chem Phys 22: 1597–1600

Harrison RJ, Redfern SAT, O'Neill HSt (1998) The temperature dependence of the cation distribution in synthetic hercynite ($FeAl_2O_4$) from in-situ neutron structure refinements. Am Mineral 83: 1092–1099

International tables for X-ray crystallography (1974), vol IV. Kynoch Press, Birmingham

Ito T, Yoshiasa A, Yamanaka T, Nakatsuka A, Maekawa H (2000) Site preference of cations and structural variation in $MgAl_{2-x}Ga_xO_4$ ($0 \le x \le 2$) spinel solid solution. Z Anorg Allg Chem 626: 42–49

Katayama I, Iseda A (2002) Thermodynamic study of spinel-type solid solutions of the Fe_3O_4–$MgFe_2O_4$ coexisting with Fe_2O_3 by emf method. Scand J Metall 31: 374–378

Katayama I, Matsuda T, Kozuka Z (1980) Thermodynamic study on Fe_3O_4–$FeCr_2O_4$ system by emf method. Osaka Univ Tech Rep 30: 385–390

Kwestroo W (1959) Spinel phase in the system MgO–Fe_2O_3–Al_2O_3. J Inorg Nucl Chem 9: 65–70

Larsson L, O'Neill HSt, Annersten H (1994) Crystal chemistry of the synthetic hercynite ($FeAl_2O_4$) from XRD structural refinements and Mössbauer spectroscopy. Eur J Mineral 6: 39–51

Maekawa H, Kato S, Kawamura K, Yokokawa T (1997) Cation mixing in natural $MgAl_2O_4$ spinel: a high-temperature ^{27}Al NMR study. Am Mineral 82: 1125–1132

Millard RL, Peterson RC, Hunter BK (1992) Temperature dependence of cation disorder in $MgAl_2O_4$ spinel using ^{27}Al and ^{17}O magic-angle spinning NMR. Am Mineral 77: 44–52

O'Neill HSt (1994) Temperature dependence of the cation distribution in $CoAl_2O_4$ spinel. Eur J Mineral 6: 603–609

O'Neill HSt, Navrotsky A (1984) Cation distributions and thermodynamic properties of binary spinel solid solutions. Am Mineral 69: 733–753

Pauling L (1960) The nature of the chemical bond, 3rd ed. Cornell University Press, Ithaca

Petrova MA, Mikirticheva GA, Novikova AS, Popova VF (1997) Spinel solid solutions in the systems $MgAl_2O_4$–$ZnAl_2O_4$ and $MgAl_2O_4$–Mg_2TiO_4. J Mater Res 12: 2584–2588

Porta P, Anichini A (1980) Distribution of cobalt ions among octahedral and tetrahedral sites in $CoGa_xAl_{2-x}O_4$ spinel solid solutions. J C S Faraday I 76: 2448–2456

Robbins M, Wertheim GK, Sherwood RC, Buchanan DNE (1971) Magnetic properties and site distributions in the system $FeCr_2O_4$–Fe_3O_4 ($Fe^{2+}Cr_{2-x}Fe^{3+}{}_xO_4$). J Phys Chem Solids 32: 717–729

Sanderson RT (1967) Inorganic chemistry. Van Nostrand-Reinhold, New York

Sasaki S (1987) RADY. A FORTRAN program for the least-squares refinement of crystal structures. National Laboratory for High Energy Physics, Japan

Shannon RD (1976) Revised effective ionic radii and systematic studies of interatomic distances in halides and chalcogenides. Acta Crystallogr (A)32: 751–767

Sharma KK, Langer K, Seifert F (1973) Some properties of spinel phases in the binary system $MgAl_2O_4$–$MgFe_2O_4$. Neues Jb Mineral Monatsh 10: 442–449

Tokonami M (1965) Atomic scattering factor for O^{2-}. Acta Crystallogr 19: 486

Toriumi K, Ozima M, Akaogi M, Saito Y (1978) Electron-density distribution in crystals of $CoAl_2O_4$. Acta Crystallogr (B)34: 1093–1096

Ulmer GC (1969) Experimental investigations of chromite spinels. In: Wilson HDB (ed) Magmatic ore deposits. Monograph 4. The Economic Geology Publishing Co, pp 114–131

Wood BJ, Kirkpatrick RJ, Montez B (1986) Order–disorder phenomena in $MgAl_2O_4$ spinel. Am Mineral 71: 999–1006